The Astrophysical Journal Letters, 759:L25 (5pp), 2012 November 1 doi:10.1088/2041-8205/759/1/L25

THE SHORTEST PERIOD sdB PLUS WHITE DWARF BINARY CD−30 11223 (GALEX J1411−3053)*

S. Vennes[1], A. Kawka[1], S. J. O'Toole[2], P. Németh[1,3], and D. Burton[4]
[1] Astronomický ústav, Akademie věd České republiky, Fričova 298, CZ-251 65 Ondřejov, Czech Republic
[2] Australian Astronomical Observatory, P.O. Box 915, 1670 North Ryde NSW, Australia
[3] Pannon Observatory and Visitor Center, 8427 Bakonybel, Hungary
[4] Faculty of Sciences, University of Southern Queensland, Toowoomba, QLD 4350, Australia
Received 2012 September 20; accepted 2012 October 2; published 2012 October 17

ABSTRACT

We report on the discovery of the shortest period binary comprising a hot subdwarf star (CD−30 11223, GALEX J1411−3053) and a massive unseen companion. Photometric data from the All Sky Automated Survey show ellipsoidal variations of the hot subdwarf primary and spectroscopic series revealed an orbital period of 70.5 minutes. The large velocity amplitude suggests the presence of a massive white dwarf in the system ($M_2/M_\odot \gtrsim 0.77$) assuming a canonical mass for the hot subdwarf ($0.48\,M_\odot$), although a white dwarf mass as low as $0.75\,M_\odot$ is allowable by postulating a subdwarf mass as low as $0.44\,M_\odot$. The amplitude of ellipsoidal variations and a high rotation velocity imposed a high-inclination to the system ($i \gtrsim 68°$) and, possibly, observable secondary transits ($i \gtrsim 74°$). At the lowest permissible inclination and assuming a subdwarf mass of $\sim 0.48\,M_\odot$, the total mass of the system reaches the Chandrasekhar mass limit at $1.35\,M_\odot$ and would exceed it for a subdwarf mass above $0.48\,M_\odot$. The system should be considered, like its sibling KPD 1930+2752, a candidate progenitor for a Type Ia supernova. The system should become semi-detached and initiate mass transfer within ≈30 Myr.

Key words: binaries: close – white dwarfs

1. INTRODUCTION

A possible scenario for triggering Type Ia supernovae involves a degenerate core collapse following the merger of two white dwarfs (see a recent summary in Ferrario 2012, and recent population syntheses by Toonen et al. 2012). A search for double-degenerate stars that could progress toward such an outcome remains unfulfilled with most binaries either too lean or too wide (SPY program, see Napiwotzki et al. 2001), with the possible exception of WD 2020−425 (Napiwotzki et al. 2005). A more promising variation on this scenario involves the interaction of a hot subdwarf star with a close white dwarf companion. Mass transferred from an He-star onto a CO white dwarf may ignite and even lead to detonation of the carbon core. At an early stage, these objects appear as AM CVn systems (see Yungelson 2008; Solheim 2010). Hot subdwarfs, also referred to as extreme horizontal branch (EHB) stars are core helium burning stars that formed preferentially in the aftermath of close, post-interacting binaries (Han et al. 2002, 2003). The identification of the short-period subdwarf plus white dwarf binary KPD 1930+2752 (Maxted et al. 2000; Geier et al. 2007) lent support to the idea, and the expectation of conservative mass transfer gave KPD 1930+2752 the character of a proper type Ia candidate progenitor. A search for other massive subluminous companions to hot subdwarf stars has so far failed to provide further candidates (MUCHFUSS program, see Geier et al. 2011, 2012b).

In this Letter, we report on the discovery of a close companion to the hot subdwarf CD−30 11223. The orbital period is the shortest known to date for such systems. The observations were carried out as part of an intermediate-dispersion survey of ∼40 hot, ultraviolet-selected subdwarf stars from the catalog of Vennes et al. (2011) and Nemeth et al. (2012) and aimed at constraining the fraction of close, evolved binaries in the EHB population. Kawka et al. (2010) described the orbital properties of the first two systems discovered as part of this survey.

The hot hydrogen-rich subdwarf (sdB) CD−30 11223 is relatively bright ($V \approx 12$) and nearby ($d = 250$–400 pc) and was first classified by Vennes et al. (2011) in spectroscopic follow-up observations of ultraviolet sources detected by the *Galaxy Evolution Explorer* (*GALEX*). Based on low-dispersion spectra, they originally determined $T_{\rm eff} = 26500 \pm 2700$ K, $\log g = 5.36 \pm 0.26$, and an abundance of helium $\log {\rm He/H} = -1.34 \pm 0.24$. These parameters were refined by Nemeth et al. (2012) using higher-dispersion spectra: $T_{\rm eff} = 30150^{+290}_{-310}$ K, $\log g = 5.72^{+0.04}_{-0.07}$, $\log {\rm He/H} = -1.58^{+0.03}_{-0.05}$. Nemeth et al. (2012) noted that temperature and surface gravity measurements in low-dispersion spectra were systematically offset from measurements obtained at higher dispersion and are probably less reliable. Moreover, Nemeth et al. (2012) reported the detection of nitrogen lines and measured an abundance $\log {\rm N/H} = -4.40^{+0.29}_{-0.67}$. They found no evidence of carbon or oxygen in the atmosphere of this star. Remarkably, large radial velocity excursions between the two series of spectra were evident and prompted further investigations. Independently, photometric variations in a large ASAS data set confirmed our suspicions that this object is in a close, evolved binary. The nature of the variations (reflection effect or tidal distortion) as well as the nature of the companion may be established with joint phasing of photometric and spectroscopic data.

In the following sections, we describe the spectroscopic and photometric data (Section 2) and their analysis (Section 3). Section 3.1 gives the results of a frequency analysis of the photometric data and Section 3.2 provides corroborating evidence of the short orbital period based on spectroscopic data. We also measured the mass function of the secondary and rotation velocity of the primary and analyzed the ellipsoidal variations to constrain the nature of the secondary star (Section 3.3). Finally, we summarize in Section 4.

2. OBSERVATIONS

The first identification spectra of the hot subdwarf CD−30 11223 were obtained with the European Southern Observatory

* Based on observations made with ESO telescopes at the La Silla Paranal Observatory under program IDs 83.D-0540, 85.D-0866, and 089.D-0864.

(ESO) Faint Object Spectrograph and Camera (EFOSC2) attached to the 3.6 m New Technology Telescope (NTT) at La Silla Observatory on UT 2009 August 24 (ESO P83 program). We used grism No. 11, which has 300 lines per mm and a blaze wavelength at 4000 Å. The slit width was set to 1 arcsec, which resulted in a spectral resolution of ∼14 Å and a coverage from 3700 to 7250 Å. We re-observed CD−30 11223 at the NTT on UT 2010 September 21 (ESO P85 program). We employed grism No. 7 (600 lines per mm) with a dispersion of 1.96 Å pixel^{-1}. The slit width was set at 1 arcsec, resulting in a resolution of ∼8 Å. Although the 2009 and 2010 spectra only offered modest velocity accuracy (50–60 km s^{-1}) the difference in measurements was close to 800 km s^{-1} suggesting the presence of a massive, close companion to the hot subdwarf. Consequently, we secured a set of intermediate-dispersion spectra, first at Siding Spring Observatory (SSO) using the 2.3 m telescope (2012 April) and at ESO using the NTT (2012 August–September).

We obtained a set of three spectra on UT 2012 April 29 and 30 with the Wide Field Spectrograph (WiFeS; Dopita et al. 2007) attached to the 2.3 m telescope at SSO. We used the B3000 and R7000 gratings which provided spectral ranges of 3200–5900 Å at a resolution $R = \lambda/\Delta\lambda = 3000$, and 5300–7000 Å at $R = 7000$, respectively. We used the RT560 dichroic beam splitter to separate the incoming light into its red and blue components. We maximized the signal to noise of each observation by extracting the spectrum from the most significant ($\lesssim$6) traces. Each trace was wavelength and flux calibrated prior to co-addition. The spectra were wavelength calibrated using NeAr arc spectra that were obtained following each observation. The exposure time was 600 s. The two exposures acquired on April 29 were separated by only 45 minutes but revealed a velocity shift close to 500 km s^{-1}.

Finally, we obtained complete orbital cycles at the NTT from UT 2012 August 30 to September 2 (ESO P89 program). We used grism No. 20 centered on Hα and with a dispersion of 0.55 Å pixel^{-1} in the spectral range from 6040 to 7140 Å. We set the slit width to 0.7 arcsec, resulting in a ∼2 Å resolution. We set the exposure times to 120 s in order to minimize orbital smearing. We obtained eight spectra on the night of August 31 and six spectra on September 1. The spectra revealed short (≈70 minutes) high-amplitude velocity variations and appeared to cover several orbits.

The field near CD−30 11223 was also covered with the All Sky Automated Survey (ASAS; Pojmanski 1997, 2001) on numerous occasions. A total of 1060 images were obtained as part of ASAS using the photometric V band. The star CD−30 11223 was not immediately identified as a variable star. We retrieved the photometric measurements using the ASAS all star catalog page.[5]

3. ANALYSIS

3.1. Photometric Frequency Analysis

The ASAS measurements span nearly 3200 days from UT 2000 December 24 to 2009 September 13. Figure 1 shows a frequency analysis of the ASAS data. Fitting a sinusoidal function to the data set unambiguously selected a signal frequency $f_{\rm phot} = 40.83377 \pm 0.00003$ day^{-1} with a semi-amplitude $\Delta m/2 = 0.047 \pm 0.004$ mag and mean magnitude $m_V = 12.342 \pm 0.003$. A reflection effect on a fainter

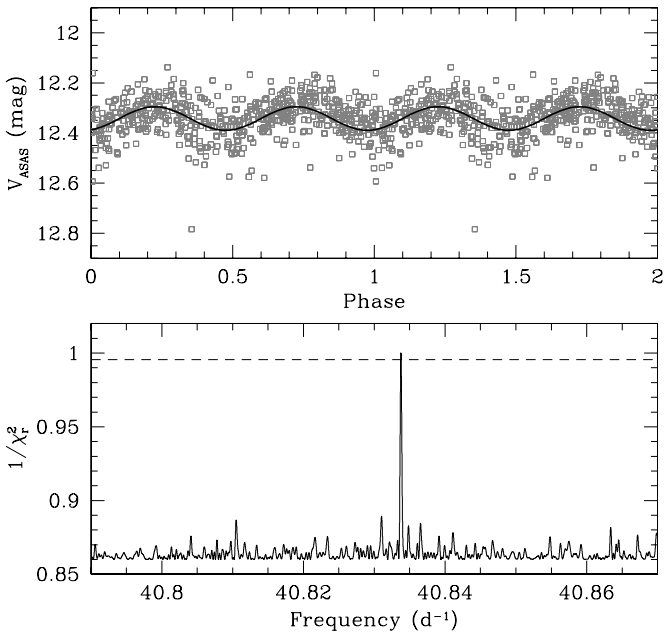

Figure 1. Bottom panel: frequency analysis of the ASAS photometric data (inverse of the normalized reduced χ^2_r vs. frequency) revealing one significant frequency near 40.83 cycles day^{-1} (full line). The 1σ significance level (horizontal dashed line) sets a formal statistical error on the chosen frequency. A weaker signal (not shown) is also present at $f_{\rm phot}/2$. Upper panel: ASAS photometric data folded on the best frequency and best fit at $f_{\rm phot}/2$.

companion would display sinusoidal variations on the orbital period $P_{\rm orb}$ ($= 2\, f_{\rm phot}^{-1}$), while tidal distortion of the primary star would induce sinusoidal variations on half the orbital period $P_{\rm orb}/2$ ($= f_{\rm phot}^{-1}$) as shown in Figure 1. An analysis of radial velocity data should help elucidate the nature of these variations.

3.2. Radial Velocities and Secondary Mass Function

All spectra were obtained at high signal-to-noise ratio and revealed well-defined Balmer and He I lines. We fitted the Hα (or Hβ in the P85 data) line cores using a Gaussian function. We estimated the errors at 50–60 km s^{-1} in the low-dispersion data (P83 and P85) and 5–10 km s^{-1} in the intermediate-dispersion data (P89 and SSO). Table 1 lists all radial velocity measurements. The heliocentric velocity is given as a function of the HJD time at mid-exposure. Folding the data on half the photometric frequency proved successful showing that the variations are due to tidal distortion of the bright hot subdwarf primary. The corresponding ephemeris is

$$P = 0.04897906 \pm 0.00000004 \text{ days}$$
$$T_0 = 1967.8426 \pm 0.0012, \quad (1)$$

where T_0 is the time of passage of the hot subdwarf primary at inferior conjunction.

Figure 2 shows the radial velocity data folded on the (above) ephemeris. The ASAS data preceded most of our radial velocity data by ∼1000 days and the accumulated error in the predicted phase is ∼1.7 minutes. In fact, our radial velocity measurements are offset from the predicted radial velocity curve by only 0.0246 phase (or ∼1.7 minutes) and firmly link the photometric variations to tidal distortion of the subdwarf primary. The residual in the more precise P89 velocity measurements is 12 km s^{-1} and is consistent with the estimated errors of 10 km s^{-1}. The velocity semi-amplitude and mean velocity

[5] http://www.astrouw.edu.pl/asas/?page=main

Table 1
Radial Velocities

Telescope	HJD (2450000+)	v_{sdB} (km s^{-1})	Telescope	HJD (2450000+)	v_{sdB} (km s^{-1})	Telescope	HJD (2450000+)	v_{sdB} (km s^{-1})
ESO NTT (P83)	5067.49158	375.7	ESO NTT (P89)	6171.46397	−296.2	ESO NTT (P89)	6171.54961	−142.9
ESO NTT (P83)	5067.49268	436.0	ESO NTT (P89)	6171.47649	225.6	ESO NTT (P89)	6172.47112	283.2
ESO NTT (P85)	5460.48093	−377.2	ESO NTT (P89)	6171.48926	339.3	ESO NTT (P89)	6172.48510	−329.0
ESO NTT (P85)	5460.48412	−313.1	ESO NTT (P89)	6171.50260	−245.3	ESO NTT (P89)	6172.49843	−61.8
SSO 2.3 m	6047.25139	−340.8	ESO NTT (P89)	6171.51655	−196.1	ESO NTT (P89)	6172.51202	415.7
SSO 2.3 m	6047.28282	145.6	ESO NTT (P89)	6171.53024	388.9	ESO NTT (P89)	6172.52588	−25.8
SSO 2.3 m	6048.01768	165.2	ESO NTT (P89)	6171.54290	161.6	ESO NTT (P89)	6172.53945	−334.2

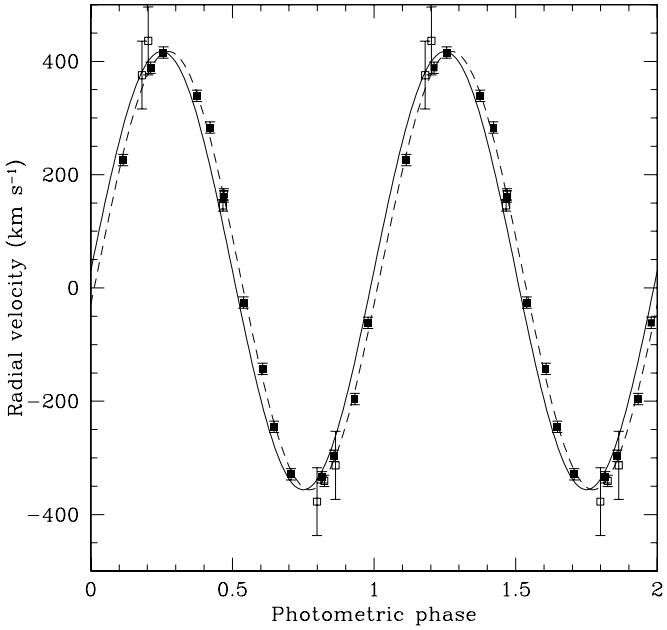

Figure 2. Radial velocity measurements (open squares: P83, P85, and SSO; full squares: P89) folded on the photometric-based ephemeris (Equation (1)) compared to the predicted radial velocity curve (full line). The velocity measurements are offset from the predicted phase by only 0.0246 (dashed line) consistent with accumulated errors in the photometric ephemeris.

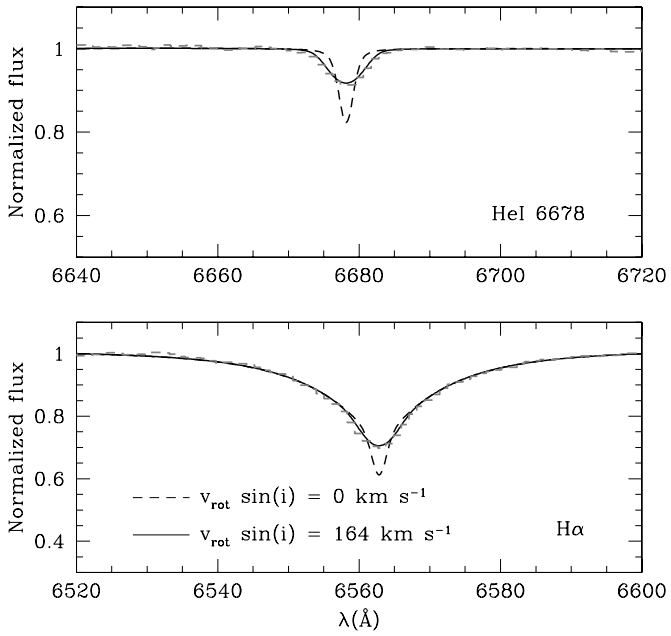

Figure 3. Co-added, intermediate-dispersion spectra (gray lines) and best-fitting, rotationally broadened synthetic spectra (full lines) near (bottom) Hα and (top) He I λ6678. The synthetic spectra without rotation broadening are shown with dashed lines. The effect of a projected rotation velocity of 164 km s^{-1} is evident in the line cores.

of the hot subdwarf are

$$\gamma_{1(\mathrm{sdB})} = 31.5 \pm 1.3 \ \mathrm{km\,s^{-1}},$$

$$K_{1(\mathrm{sdB})} = 386.9 \pm 1.9 \ \mathrm{km\,s^{-1}},$$

and the corresponding mass function for the unseen companion is

$$f_2 = 0.294 \pm 0.004 \, M_\odot.$$

Finally, we generated a phase-corrected, co-added spectrum of the Hα and He I λ6678 using all ESO P89 spectra. The exposure time limited orbital smearing to $\lesssim$50 km s^{-1}, or nearly half of the spectral resolution of the P89 data (90 km s^{-1}). A rotation velocity comparable or in excess of 100 km s^{-1} should be readily measurable.

3.3. Properties of the Primary and Nature of the Secondary

Approximating the full amplitude of the ellipsoidal variations by (see Warner 1995)

$$\Delta m = 3.5\, q \left(\frac{R_1}{a}\right)^3 \sin^2 i,$$

where $q = M_1/M_2$, M_1, and R_1 are the mass and radius of the hot subdwarf primary, and M_2 is the mass of the unseen companion. The subdwarf mass is constrained independently but M_2 and i are treated as free parameters. The semimajor axis a follows Kepler's third law. The gravity darkening and limb darkening coefficients were held fixed at values suggested by Warner (1995), e.g., $\mu_g = 1$ and $\mu = 0.36$.

The subdwarf radius may be obtained from $R_1/R_\odot = \sqrt{M_1/(g/g_\odot)}$. Adopting $\log g$ from Nemeth et al. (2012) and assuming $M_1 = 0.48\, M_\odot$, we estimated the subdwarf radius $R_1 = 0.159^{+0.13}_{-0.07}\, R_\odot$. We may also set an independent and more reliable constraint on the primary radius using a measurement of the rotation velocity (Figure 3). Fitting synthetic Hα profiles to co-added P89 spectra and adopting best-fit model parameters (Nemeth et al. 2012) we measured $v_{\mathrm{rot}} \sin i = 164 \pm 5$ km s^{-1}. The models were first convolved with a Gaussian function with an FWHM set at 2 Å. Also, the effect of orbital smearing was taken into account by smoothing the models with a box-car function with a full width of 50 km s^{-1}. Geier & Heber (2012) found that all subdwarfs from their sample, single or in binaries with a period longer than 1.2 days, are slow rotators ($v_{\mathrm{rot}} \sin i \lesssim$ 10 km s^{-1}). Clearly, CD−30 11223 is exceptional. We verified our solution by convolving with the rotation broadening function

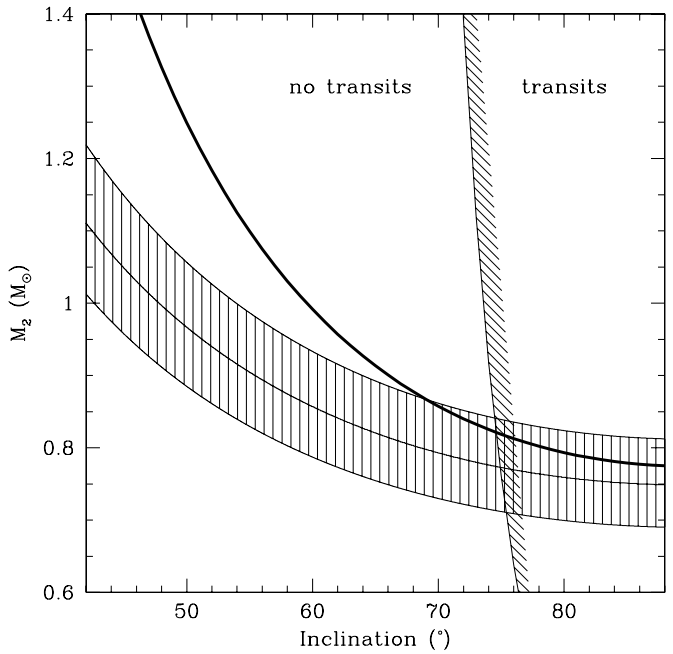

Figure 4. Constraints on the secondary mass (M_2) as a function of the orbital inclination. First, M_2 is obtained from the measured mass function f_2 assuming $M_1/M_\odot = 0.48$ (thick full line). The range of primary mass is dictated by evolutionary considerations, such as the evolutionary tracks of Dorman et al. (1993) that generates remnants of 0.48 $M_\odot$ (Zhang et al. 2009; Fontaine et al. 2012). Next, a relation between M_2 and the inclination is derived from the measured amplitude of the ellipsoidal variations assuming $M_1 = 0.48$ (thin lines from bottom to top $\Delta m = 0.086, 0.094, 0.102$ mag and shaded area). The diagram is split between areas with detectable and non-detectable transits.

a template built using a subdwarf (GALEX J0206+1438) similar to CD−30 11223 and observed with the same setup. We measured an identical value of $v_{\rm rot} \sin i = 164 \pm 15$ km s^{-1} but with larger error bars possibly because of a slight parameter mismatch between the two stars. Taking observed ellipsoidal variations as evidence that the subdwarf is tidally locked to the primary, the rotation and orbital velocities are related:

$$\frac{v_{\rm rot} \sin i}{K_1} = \frac{R_1}{a_1},$$

and since $a = a_1 + a_2 = a_1(1+q)$, then

$$R_1 = \frac{a}{1+q} \frac{v_{\rm rot} \sin i}{K_1},$$

where $q = M_1/M_2 = a_2/a_1$. The resulting primary radius is consistent with the gravitational radius (0.159 $R_\odot$) for all probable inclinations ($\gtrsim$50°).

Figure 4 shows a set of constraints placed on the free parameters M_2 and i. The mass function defines a narrow constraint for a given subdwarf mass: the minimum secondary mass ranges from 0.75 to 0.77 $M_\odot$ for a subdwarf mass ranging from 0.44 to 0.48 $M_\odot$. Combining mass function and tidal constraints at $M_1 = 0.48\,M_\odot$, the secondary mass ranges from 0.77 to 0.87 $M_\odot$, implying a total mass of 1.25–1.35 $M_\odot$. The effective temperature and surface gravity of CD−30 11223 place it squarely among the bulk of sdB stars that are best described with the models of Dorman et al. (1993) within a narrow mass range centered on ∼0.48 $M_\odot$. Moreover, tests showed that constraints placed by ellipsoidal variations and by the mass function are incompatible below $M_1/M_\odot \approx 0.44$. Therefore, assuming a mass close to 0.48 $M_\odot$ is probably justified and the possibility that past interactions may have left an extremely low-mass remnant (≈0.3 $M_\odot$; see, e.g., Heber et al. 2003) does not need to be considered.

Uncertainties on the rotation velocity measurements are possibly affected by systematic effects such as over- or under-estimated spectral resolution or orbital smearing. Assuming a rotation velocity as low as 150 km s^{-1} would increase the upper mass limit to 1.05 $M_\odot$ and push the inclination as low as 57°.

The possibility of shallow ($\Delta m \approx (R_2/R_1)^2 \lesssim 5$ mmag) secondary transits cannot be ruled out and transit timing would allow us to constrain accurately the inclination and stellar radii. Transits may become observable at an inclination i such that $\tan(90^\circ - i) \lesssim R_1/a$ or $i \gtrsim 74^\circ$ (where $a \approx 0.6\,R_\odot$). It is worth noting that all solutions provide a primary radius smaller than its Roche lobe radius ($R_L \approx 0.2\,R_\odot$), excluding the possibility of present-day interaction.

4. SUMMARY AND CONCLUSIONS

We found that the hot subdwarf CD−30 11223 is in a close 70.5 minute binary with an unseen companion presumed to be a white dwarf. The orbital properties and noted photometric variations suggest the presence of a companion with a minimum mass of 0.75 $M_\odot$ assuming a minimum mass of 0.44 $M_\odot$ for the primary. However, the measured parameters of the sdB CD−30 11223 favor a canonical mass close to 0.48 $M_\odot$ that would correspond to a minimum mass of 0.77 $M_\odot$ for the secondary. Constraining the radius of the primary using a measurement of its rotation velocity and fitting the amplitude of the ellipsoidal variations set an upper limit of 0.87 $M_\odot$ for the secondary mass at an inclination $i \approx 68^\circ$ and a total mass of 1.35 $M_\odot$ for the system. However, systematic effects in the measurement of the rotation velocity and the possibility that the primary mass may exceed 0.48 $M_\odot$ imply that the system mass may exceed the Chandrasekhar mass limit ($M_{\rm Ch}$). Observations of transits would help constrain the inclination of the system and the primary radius.

Following Ritter (1986), the system will initiate mass transfer in 25–28 Myr with a contact period of 49 minutes. While transferring mass, the system would take the appearance of an AM CVn system that could eventually trigger a Type Ia supernova (Yungelson 2008; Solheim 2010). With a total lifetime on the EHB that must exceed 100 Myr (Dorman et al. 1993) and the short time remaining before contact ($\lesssim$30 Myr), it is likely that a substantial amount of helium may remain in the envelope of the EHB star that would then constitute a generous helium donor. Following Nelemans et al. (2001), the outcome depends on the mass of the accreting white dwarf and the amount of helium available from the donor. The minimum mass of the white dwarf ($\gtrsim$0.75 $M_\odot$) exceeds a threshold (0.6 $M_\odot$) below which the system would undergo nova-like, helium-flash episodes. Instead, should enough helium ($\gtrsim$0.3 $M_\odot$) accumulate on the massive white dwarf after the onset of stable mass transfer the system may suffer helium detonation that could light-up the C/O core, triggering a Type Ia supernova. On the other hand, it is possible that the EHB star could exhaust most of its helium supply before contact and merge with its massive white dwarf companion. Should the total mass of the system exceed $M_{\rm Ch}$, the remnant could also trigger a Type Ia supernova. Alternatively, should the system mass prove insufficient, the immediate outcome would be a hot, ultramassive white dwarf such as those sampled by Vennes et al. (1997) in the *Extreme Ultraviolet Explorer* survey.

We note that Geier et al. (2012a) independently reported on this system and reached similar conclusions.

S.V. and A.K. acknowledge support from the Grant Agency of the Czech Republic (GA ČR P209/10/0967, GA ČR P209/12/0217). This work was also supported by the project RVO:67985815 in the Czech Republic. We thank the referee for helping us clarify the evolutionary prospects of the system. Also, we thank A. Williams (Perth Observatory) for his contribution to the project.

Note added in proof. L. Yungelson informed us that, following Fink et al. (2010), a supernova may be triggered by an accreted mass of helium as low as $0.1\,M_{\odot}$ for a $0.8\,M_{\odot}$ white dwarf, thereby increasing the odds of such an event taking place in CD−30 11223.

REFERENCES

Dopita, M., Hart, J., McGregor, P., et al. 2007, Ap&SS, 310, 255
Dorman, B., Rood, R. T., & O'Connell, R. W. 1993, ApJ, 419, 596
Ferrario, L. 2012, in IAU Symp. 281, Binary Paths to Type Ia Supernovae Explosions, ed. R. Di Stefano, M. Orio, & M. Moe (Cambridge: Cambridge Univ. Press), in press (arXiv:1209.1201v1)
Fink, M., Röpke, F. K., Hillbrandt, W., et al. 2010, A&A, 514, 53
Fontaine, G., Brassard, P., Charpinet, S., et al. 2012, A&A, 539, A12
Geier, S., & Heber, U. 2012, A&A, 543, A149
Geier, S., Hirsch, H., Tillich, A., et al. 2011, A&A, 530, A28
Geier, S., Marsh, T. R., Dunlap, B. H., et al. 2012a, in ASP Conf. Ser., 18th European White Dwarf Workshop, ed. J. Krzesinski, G. Stachowski, & P. Moskalik (San Francisco, CA: ASP), in press (arXiv:1209.4740v1)
Geier, S., Nesslinger, S., Heber, U., et al. 2007, A&A, 464, 299
Geier, S., Schaffenroth, V., Hirsch, H., et al. 2012b, Astron. Nachr., 333, 431
Han, Z., Podsiadlowski, P., Maxted, P. F. L., & Marsh, T. R. 2003, MNRAS, 341, 669
Han, Z., Podsiadlowski, P., Maxted, P. F. L., Marsh, T. R., & Ivanova, N. 2002, MNRAS, 336, 449
Heber, U., Edelmann, H., Lisker, T., & Napiwotzki, R. 2003, A&A, 411, L477
Kawka, A., Vennes, S., Németh, P., Kraus, M., & Kubát, J. 2010, MNRAS, 408, 992
Maxted, P. F. L., Marsh, T. R., & North, R. C. 2000, MNRAS, 317, L41
Napiwotzki, R., Christlieb, N., Drechsel, H., et al. 2001, Astron. Nachr., 322, 411
Napiwotzki, R., Karl, C. A., Nelemans, G., et al. 2005, in ASP Conf. Ser. 334, 14th European Workshop on White Dwarfs, ed. D. Koester & S. Moehler (San Francisco, CA: ASP), 375
Nelemans, G., Portegies Zwart, S. F., Verbunt, F., & Yungelson, L. R. 2001, A&A, 368, 939
Németh, P., Kawka, A., & Vennes, S. 2012, MNRAS, in press
Pojmanski, G. 1997, Acta Astron., 47, 467
Pojmanski, G. 2001, in ASP Conf. Ser. 246, IAU Colloq. 183, Small Telescope Astronomy on Global Scales, ed. B. Paczynski, W.-P. Chen, & C. Lemme (San Francisco, CA: ASP), 53
Ritter, H. 1986, A&A, 169, 139
Solheim, J.-E. 2010, PASP, 122, 1133
Toonen, S., Nelemans, G., & Portegies Zwart, S. 2012, A&A, 546, A70
Vennes, S., Kawka, A., & Németh, P. 2011, MNRAS, 410, 2095
Vennes, S., Thejll, P. A., Galvan, R. G., & Dupuis, J. 1997, ApJ, 480, 714
Warner, B. 1995, Cataclysmic Variable Stars (Cambridge Astrophysics Series, Vol. 28; Cambridge: Cambridge University Press)
Yungelson, L. R. 2008, Astron. Lett., 34, 620
Zhang, X., Chen, X., & Han, Z. 2009, A&A, 504, L13